Supporting Information

Membrane Allostery and Unique Hydrophobic Sites Promote Enzyme Substrate Specificity

Varnavas D. Mouchlis*, Yuan Chen, J. Andrew McCammon and Edward A. Dennis*

Department of Chemistry and Biochemistry and Department of Pharmacology, School of Medicine, University of California, San Diego, La Jolla, California 92093-0601

Corresponding Authors
*E-mail: vmouchlis@gmail.com.
*E-mail: edennis@ucsd.edu. Phone: +1 858 534 3055.

Table of Contents

Supplementary Methods

Lipidomics HPLC/MS High-Throughput Assay

Assaying PLA_2 activity. Group specific assays were employed to determine the activity of human recombinant Group IVA cytosolic ($cPLA_2$), Group VIA calcium-independent ($iPLA_2$) and Group V secreted ($sPLA_2$) phospholipases A_2 in a mixed micelle 96 well-plate assay. The substrate for each enzyme consisted of 100 μM of phospholipid, 400 μM of C12E8 surfactant in a 1:4 ratio (see Figure S3), and 2.5 μM of 17:0 LPC as an internal standard. For $cPLA_2$, the total phospholipid concentration (100 μM) consisted of 97 μM phospholipid substrate and 3 μM of PI(4,5)P2 which enhances the activity of the enzyme. A specific buffer was prepared to achieve optimum conditions for each enzyme's activity. The buffer for $cPLA_2$ contained 100 mM HEPES pH 7.5, 90 μM $CaCl_2$, and 2 mM DTT. For $iPLA_2$, the buffer consisted of a 100 mM HEPES pH 7.5, 2 mM ATP, and 4 mM DTT. Finally, the buffer for $sPLA_2$ contained 50 mM Tris-HCl pH 8.0 and 5 mM $CaCl_2$. The enzymatic reaction was performed in a 96 well-plate using a Benchmark Scientific H5000-H MultiTherm heating shaker for 30 min at 40 °C. Each reaction was quenched with a 120 μL of methanol/acetonitrile (80/20, v/v), and the samples were analyzed using the HPLC-MS system. A blank experiment, which did not contain enzyme, was also included for each substrate to determine the non-enzymatic hydrolysis product and to detect any changes in the intensity of the 17:0 LPC internal standard. All experiments were performed in triplicate and the calculated standard deviation is included in each graph with error bars.

*HPLC-MS/MS***.** A Shimadzu HPLC system consisting of a system controller (SCL-10Avp) with two HPLC pumps (LC-10ADvp), a CTC Analytics PAL autosampler platform (Leap Technologies), and a column controller instrument (Analytical Sales & Products, Inc) were employed for liquid chromatographic analysis. Mass spectrometric analysis was performed using an AB Sciex 4000 QTRAP triple quadrupole/linear ion trap hybrid mass spectrometer equipped with a Turbo V ion source.

Hydrophilic interaction chromatography (HILIC). A Phenomenex Kinetex® 2.6 μm HILIC 100 Å column of 30×2.1 mm size was used for HPLC separation. The binary gradient consisted of (A) ACN/water (95/5, v/v, pH=8.0) containing 25 mM $AcNH_4$ and (B) ACN/water (50/50, v/v, pH=7.5) containing 25 mM $AcNH_4$. Gradient elution was carried out for 1.6 min at a flow rate of 0.8 mL/min. Gradient conditions were as follows: 0% B for 0.8 min; 0-100% B for 0.4 min; 100% B for 0.3 min; and 100%B for 0.1 min. A 10 µL aliquot of each sample was injected into the column. The column temperature was kept at 40 °C. All samples were maintained at 4 °C throughout the analysis.

Mass Spectrometry. Lysophospholipids (primary and internal standards), phospholipids and surfactant (C12E8) were detected in positive electrospray ionization (ESI) mode, while arachidonic acid (AA) in negative ESI mode. Molecular species were detected as $[M+H]^+$ ions in

positive ion mode and as $[M-H]^-$ ions in negative ion mode. Curtain gas (CUR), nebulizer gas (GS1), and turbo-gas (GS2) were set to 10 psi, 50 psi and 20 psi, respectively. The electrospray voltage was set to +4.5 kV or -4.5 kV, and the turbo ion spray source temperature was set to 500 °C. Lysophospholipids were analyzed using scheduled multiple reaction monitoring (MRM). Declustering potentials and collision energies were optimized for each analyte to achieve optimal mass spectrometric detection. Nitrogen was employed as the collision gas. Data acquisitions were performed using Analyst software. MultiQuant software was used to quantify all metabolites.

Preparation of standard curves. Standard curves were generated for lysophospholipid analytes (also known as primary standards) including 16:0 and 18:0 LPA, 16:0 and 18:0 LPC, 16:0 and 18:0 LPE, 16:0 and 18:0 LPG, 16:0 and 18:0 LPS (Figure S2). 17:0 LPC was used as an internal standard for each primary standard. Several concentrations in methanol/acetonitrile (80/20, v/v) of each primary standard were used to generate each standard curve. 200 μL of each concentration was transferred in a DP vial and the internal standard (17:0 LPC) was added at a final concentration of 2.5 μM.

Reagents. Phospholipids, primary standards, and internal standards were purchased from Avanti® Polar Lipids, Inc. Optima® LC-MS grade acetonitrile (ACN), water (H_2O), and HPLC grade ammonium acetate ($AcNH_4$) were obtained from Fisher Scientific. Octaethylene glycol monododecyl ether (C12E8) was obtained from Sigma-Aldrich.

Molecular Dynamics (MD) simulations

Enzyme-substrate complexes. Initial complexes of each enzyme with PAPE, PAPS, PLPC, and PMPC were generated using the crystal structure of $cPLA_2$,[1] a previously published homology model of $iPLA_2$ based on patatin,[2] and a homology model of GV $sPLA_2$ based on GIIA $sPLA_2$. GV $sPLA_2$ has 47% identities and 61% homology with GIIA $sPLA_2$ for which a crystal structure is available. The homology model of GV $sPLA_2$ was built using the Prime software implemented in Schrödinger suite 2017 (see Figure S11A).[3] Phospholipids were docked in the active site of each enzyme using the Glide software implemented in Schrödinger suite 2017 using a previously published docking protocol.[4-6]

Enzyme-membrane systems. The Membrane Builder implemented in CHARMM-GUI was employed to generate enzyme-membrane models for the MD simulations.[7-8] The membrane patch consisted of POPC, SAPC, POPE, POPA, POPG, POPS, SAPI(4,5)P2, and cholesterol. The average ratios of the lipids were chosen to be 0.48 for PC, 0.27 for PE, 0.10 for PI(4,5)P2, 0.06 for PS, and 0.09 for PA and PG. The average cholesterol/lipid ratio was chosen to be 0.40. These ratios are the average ratio of the nuclear, mitochondrial, and plasma membranes where $cPLA_2$, $iPLA_2$ and $sPLA_2$ are localized, respectively.[9] The membrane composition was selected based on the localization of each enzyme on cellular membranes according to previously published

studies.[10-12] Each system was solvated with TIP3P water molecules and neutralized with 150 mM sodium chloride (NaCl) using the Visual Molecular Dynamics (VMD) package (see Figure S11B).[13]

Equilibration and production runs. Molecular dynamics simulations were carried out using NAMD 2.12.[14] The following minimization and equilibration protocol was performed: a minimization of 80,000 steps was initially performed by applying harmonic constraints on the enzyme-ligand-membrane that were gradually turned off using a constraint scaling factor, followed by a second 120,000 steps minimization without constraints. An initial equilibration of 10,000 steps was performed by also applying harmonic constraints on the enzyme-ligand-membrane that were gradually turned off using the same constraint scaling factor, followed by a second 10,000 steps equilibration without constraints. During the equilibration, each system was slowly heated and held to 310 K using temperature reassignment with a reassignment frequency of 500 timesteps (1000 fs) and a reassignment increment of 1 K. The above minimization and equilibration protocol was sufficient to induce the appropriate disorder of a fluid-like bilayer, avoid unnatural atomistic positions, and failure of the simulations by atoms moving at very high velocities. Each system was finally subjected to a 1 μs production run. For each production run, the temperature was maintained at 310 K using the Langevin thermostat with Langevin coupling coefficient of 1/ps.[15] The *NPT* ensemble was employed and the pressure was kept constant at 1.01325 kPa using the Langevin piston method with the "useGroupPressure", "useFlexibleCell", and "useConstantArea" parameters turned on.[16] A time step of 2 fs was used in combination with the SHAKE algorithm to hold the bonds of hydrogen atoms similarly constrained.[17] Nonbonded interactions and full electrostatics were calculated every 1 and 2 time steps, respectively. Switching functions are used to smoothly take electrostatic and van der Waals interactions to zero with a switching distance of 10 Å and a cutoff of 12 Å. Long-range electrostatic forces in the periodic system were evaluated using the Particle Mesh Ewald (PME) Sum method with grid spacing 1/Å.[18] The CHARMM General Force Field (CGenFF) and the CHARMM36 all-atom additive force field and parameters were used for the simulations.[19-20]

Binding pocket volume calculations. POVME algorithm was employed for calculating the volume of the binding pocket of each enzyme over the time of each simulation.[21] A total number of 6,252 frames from each simulation trajectory was used for the calculations. The frames were aligned on the initial complex that was used to carry out the simulation using VMD and were saved in multi-frame PDB format. To define the "inclusion sphere" that entirely encloses the binding pocket of each enzyme, the center of mass of the residues within 5 Å around the bound phospholipid molecule was used as the x, y, z coordinates of the sphere. An "inclusion sphere" radius of 11 Å was used. Equidistant points were generated in POVME using a grid spacing of 1 Å and a distance cutoff of 1.09 Å.

Supplementary Figures

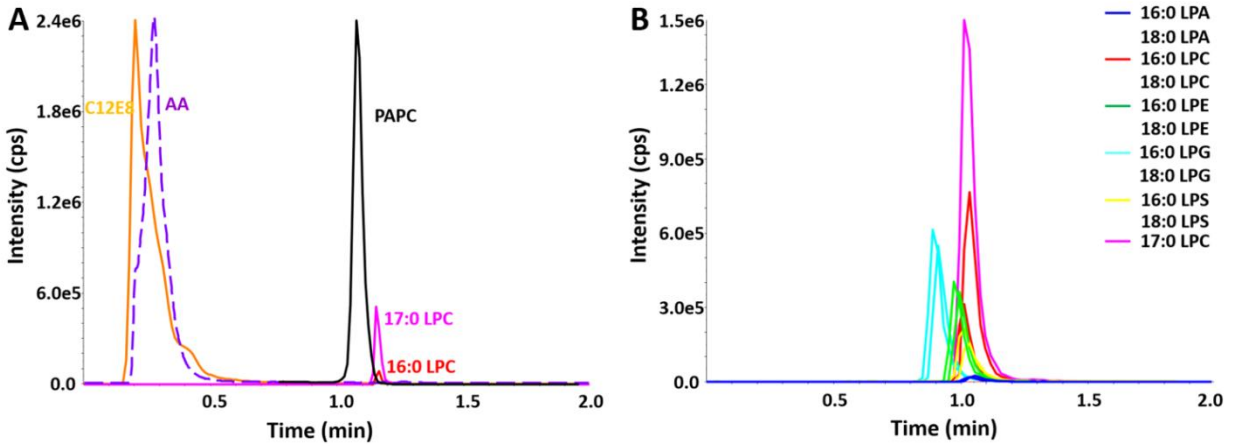

Figure S1. Chromatographic separation by HILIC HPLC and peak monitoring by MRM. (A) Chromatographically separated peaks of the PLA_2 mixed micelle assay components: $C_{12}E_8$, PAPC, 16:0 LPC, and 17:0 LPC were measured in positive ion mode while AA was measured in negative ion mode, and (B) chromatographically separated MRM peaks for all lysophospholipid analytes.

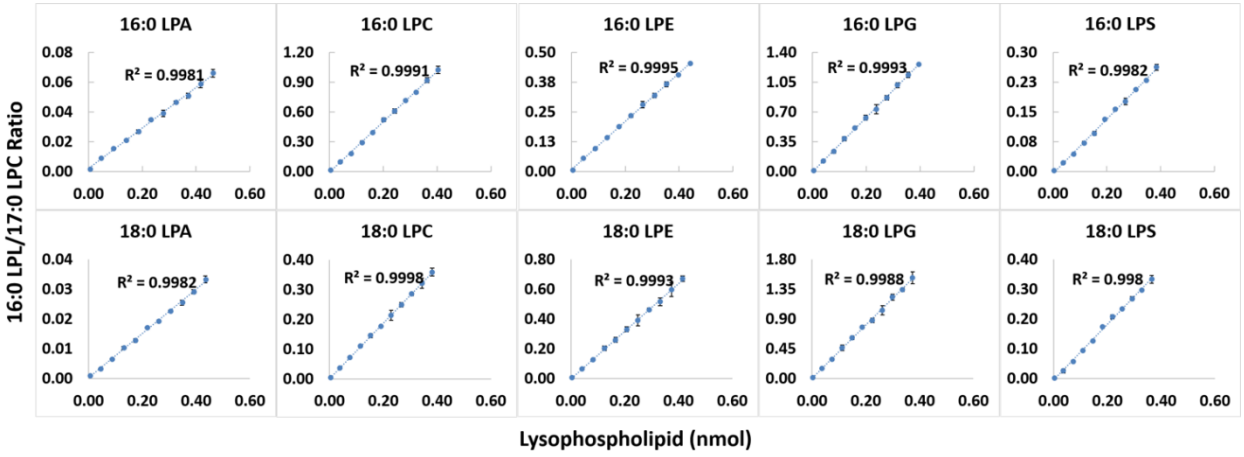

Figure S2. Standard curves for lysophospholipid analytes including 16:0 and 18:0 LPA, 16:0 and 18:0 LPC, 16:0 and 18:0 LPE, 16:0 and 18:0 LPG, and 16:0 and 18:0 LPS as a ratio to the internal standard 17:0 LPC.

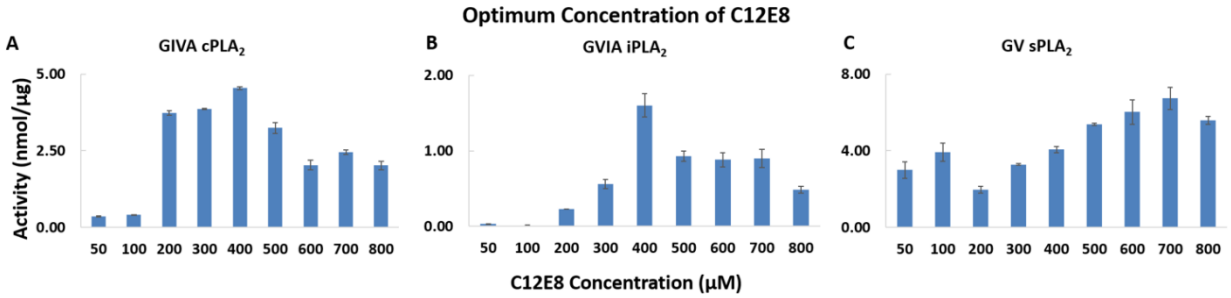

Figure S3. Enzyme activity toward 100 μM PAPC in mixed micelles with varying concentrations of C12E8 surfactant for (A) $cPLA_2$, (B) $iPLA_2$, and (C) $sPLA_2$.

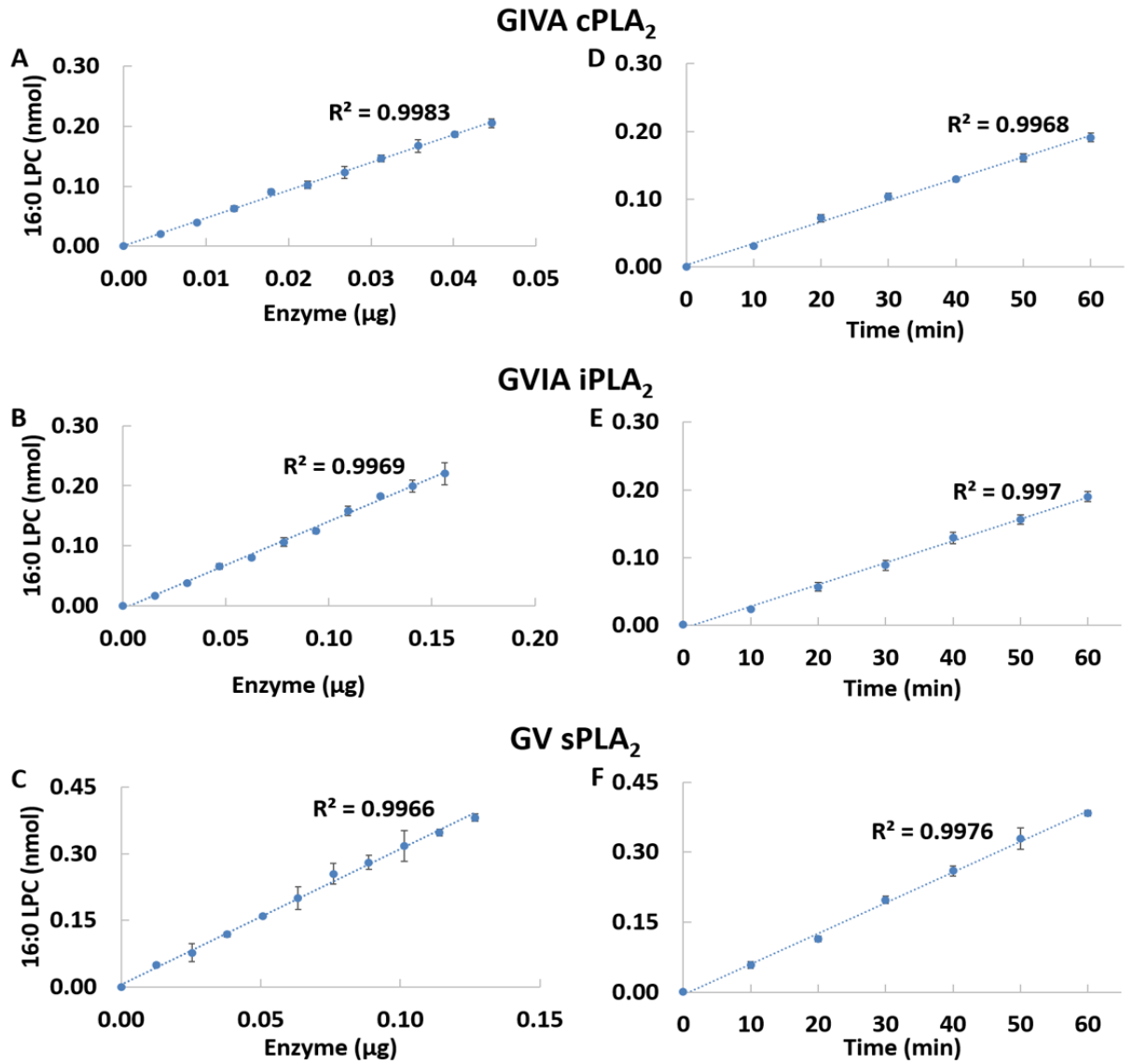

Figure S4. Product formed as a function of the amount of enzyme for (A) $cPLA_2$, (B) $iPLA_2$, and (C) $sPLA_2$. Product formed as a function of time for (D) $cPLA_2$, (E) $iPLA_2$, and (F) $sPLA_2$.

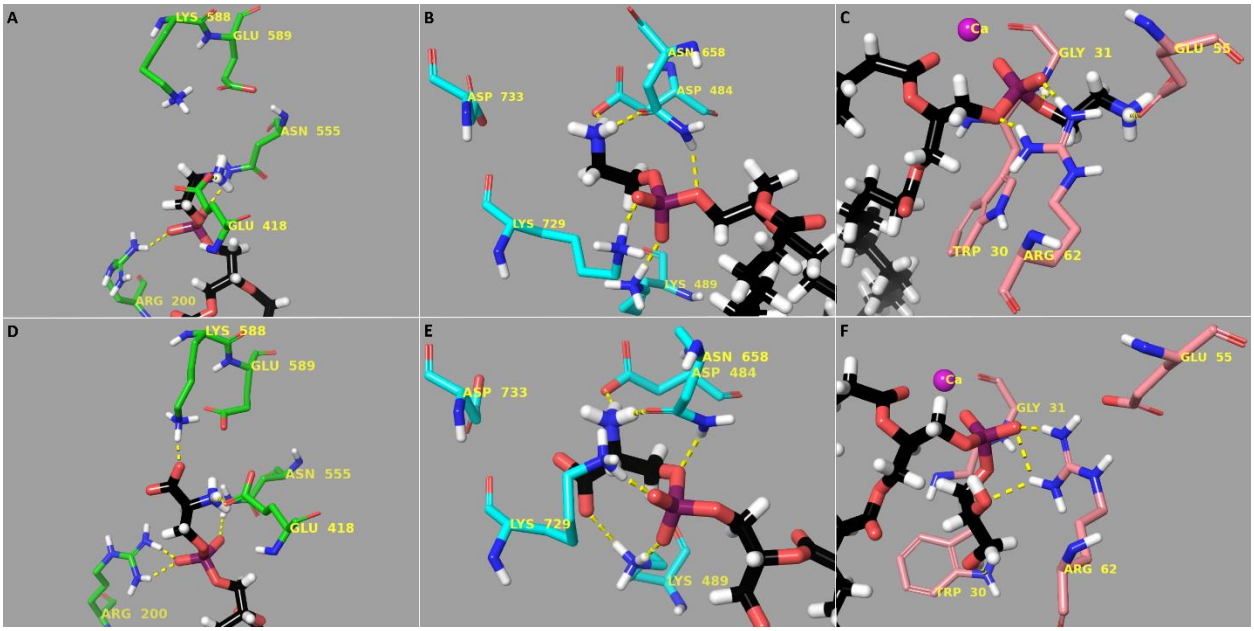

Figure S5. Interactions of phosphatidylethanolamine (PE) with the catalytic residues of (A) $cPLA_2$ (Movie 1), (B) $iPLA_2$ (Movie 5), and (C) $sPLA_2$ (Movie 9). Interactions of phosphatidylserine (PS) with the active site residues of (D) $cPLA_2$ (Movie 2), (E) $iPLA_2$ (Movie 6), and (F) interactions of phosphatidylglycerol (PG) with the active site residues of $sPLA_2$ (Movie 10).

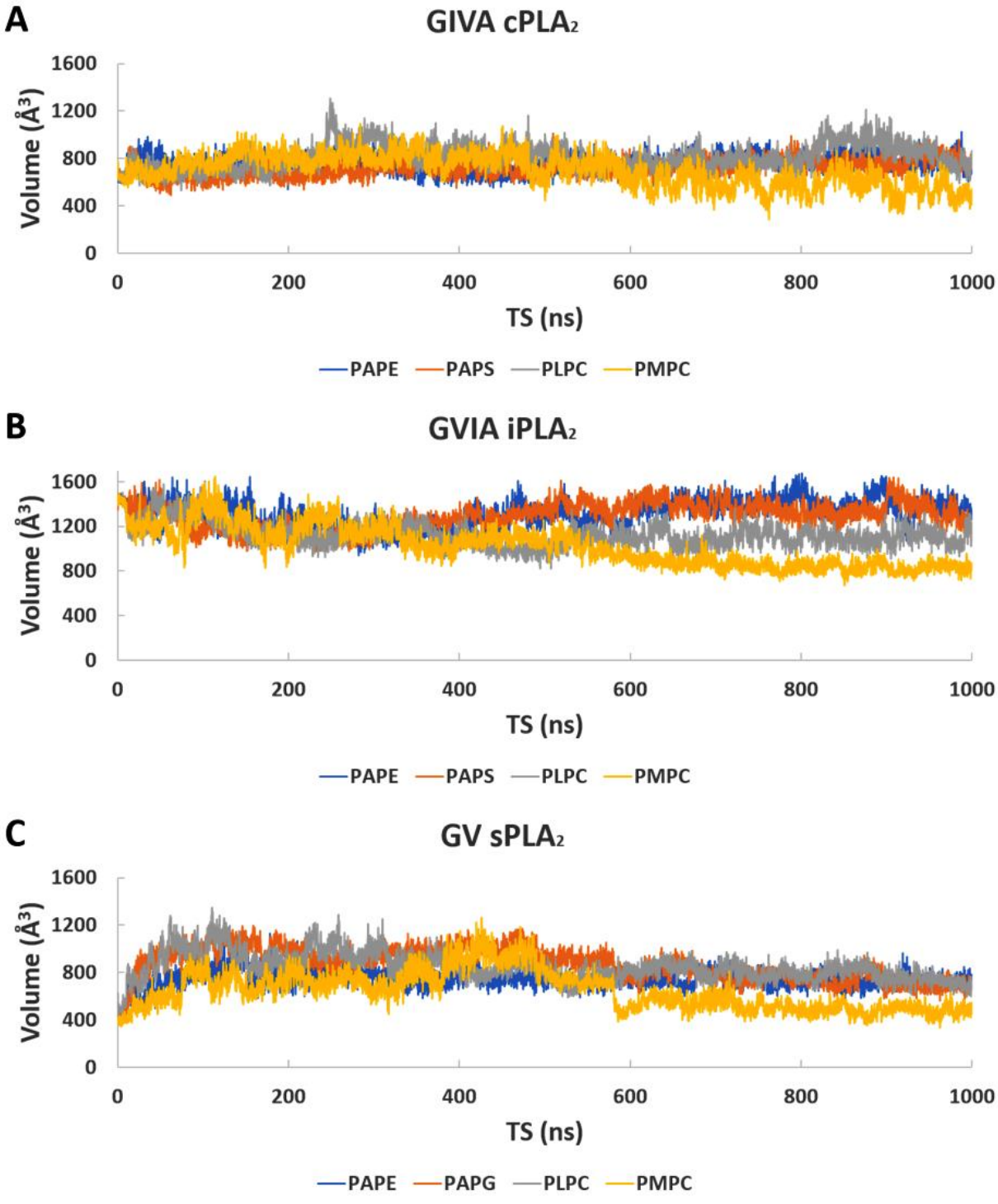

Figure S6. Active site volume during the time of the simulation in the presence of PAPE (blue), PAPS or PAPG (orange), PLPC (gray), and PMPC (yellow) for (A) $cPLA_2$, (B) $iPLA_2$, and (C) $sPLA_2$.

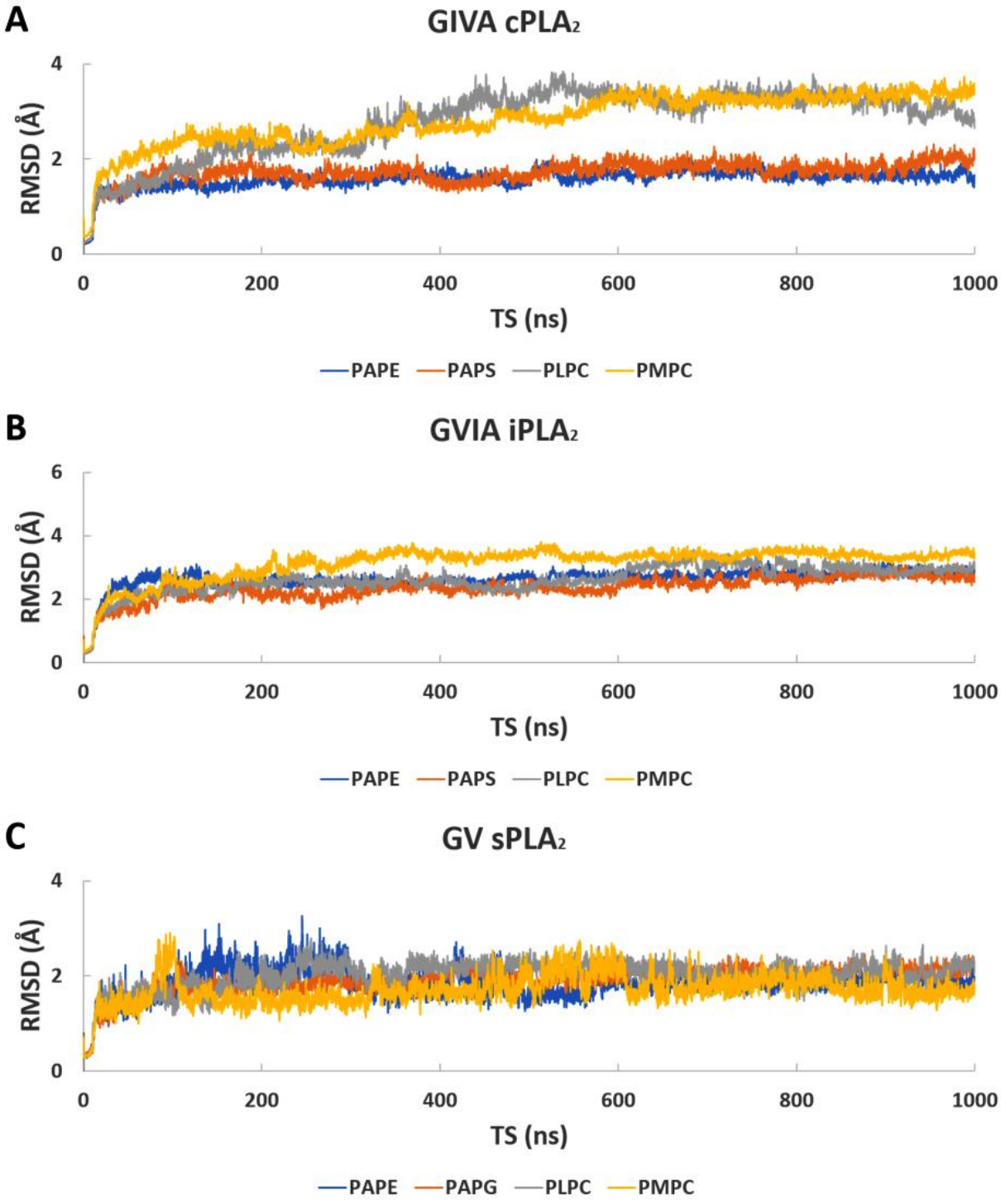

Figure S7. The root-mean-square deviation (RMSD) of the enzyme backbone atoms during the time of the simulation in the presence of PAPE (blue), PAPS or PAPG (orange), PLPC (gray), and PMPC (yellow) for (A) $cPLA_2$, (B) $iPLA_2$, and (C) $sPLA_2$.

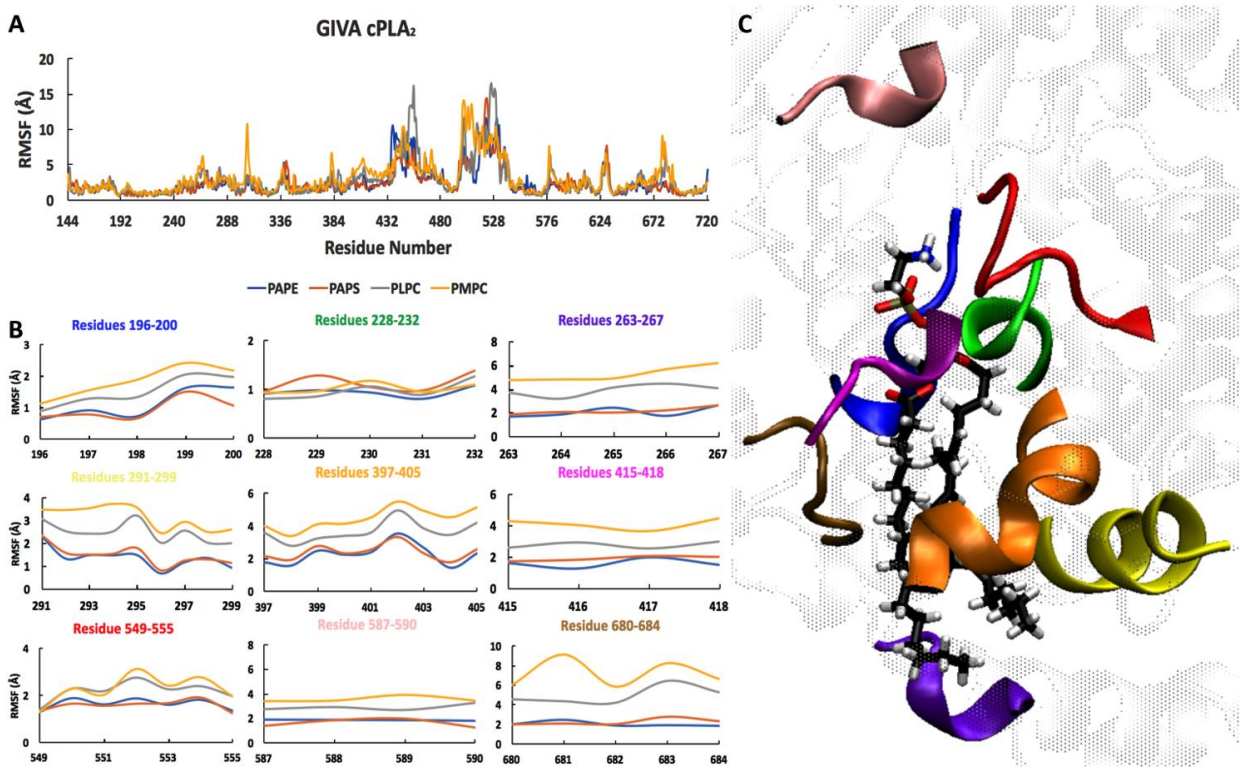

Figure S8. Flexibility of $cPLA_2$ during the simulation in the presence of PAPE (blue), PAPS (orange), PLPC (gray), and PMPC (yellow) based on root-mean-square fluctuation (RMSF) data. (A) RMSF for all residues of $cPLA_2$, (B) RMSF for residues on regions 4 Å around the phospholipid molecule, and (C) visual representation of the regions in section B.

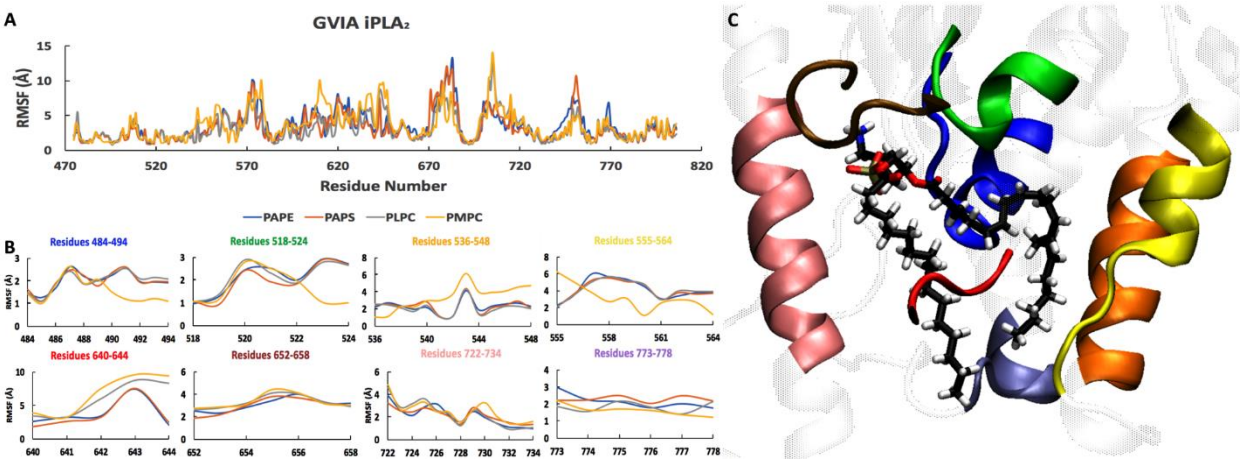

Figure S9. Flexibility of $iPLA_2$ during the simulation in the presence of PAPE (blue), PAPS (orange), PLPC (gray), and PMPC (yellow) based on root-mean-square fluctuation (RMSF) data. (A) RMSF for all residues of $cPLA_2$, (B) RMSF for residues on regions 4 Å around the phospholipid molecule, and (C) visual representation of the regions in section B.

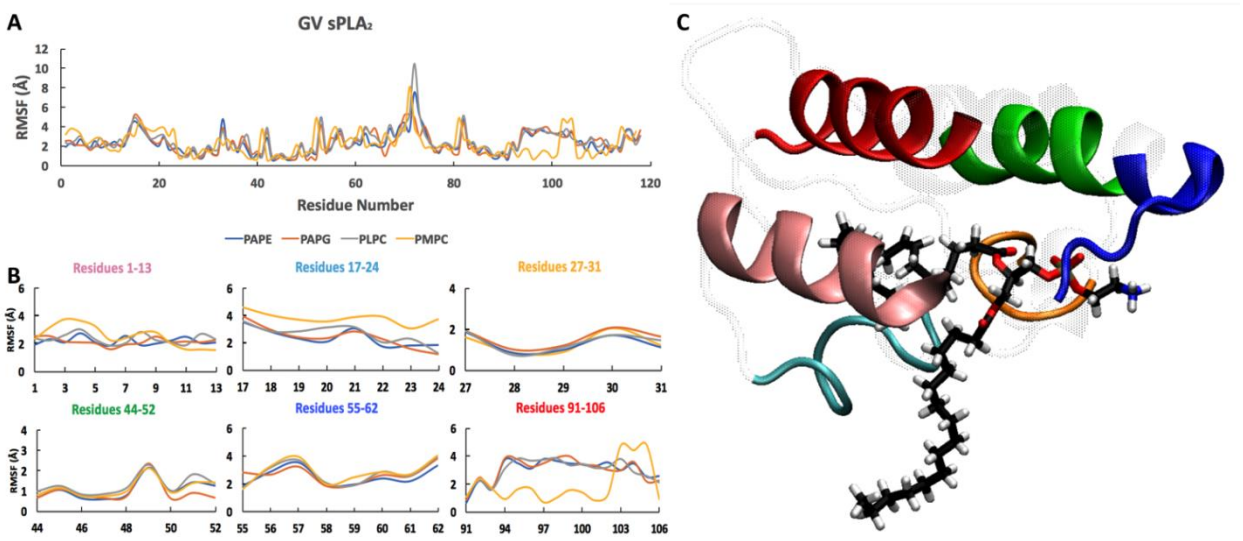

Figure S10. Flexibility of $sPLA_2$ during the simulation in the presence of PAPE (blue), PAPG (orange), PLPC (gray), and PMPC (yellow) based on root-mean-square fluctuation (RMSF) data. (A) RMSF for all residues of $cPLA_2$, (B) RMSF for residues on regions 4 Å around the phospholipid molecule, and (C) visual representation of the regions in section B.

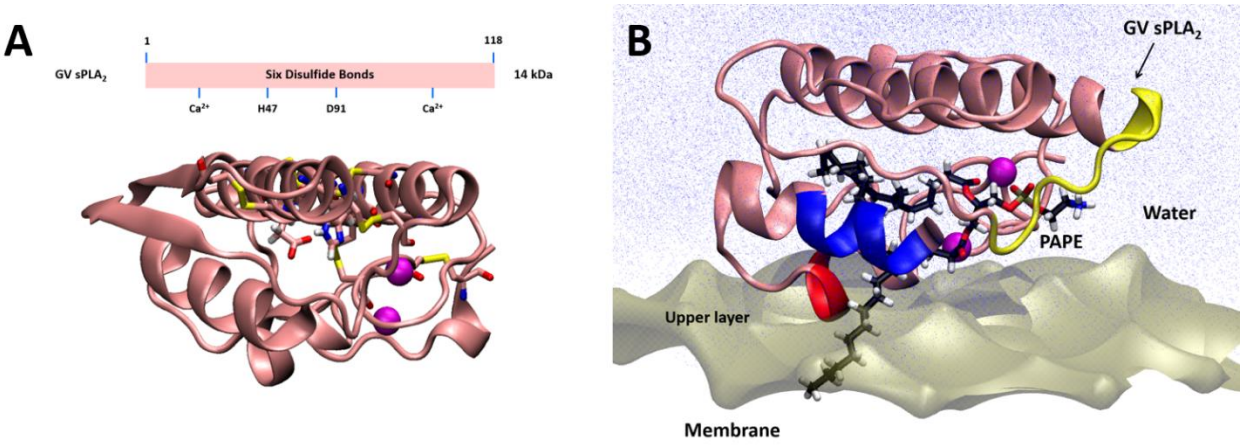

Figure S11. Three-dimensional models for GV $sPLA_2$. (A) Enzyme homology model based on the X-ray crystal structure of GIIA $sPLA_2$, and (B) enzyme-PAPE complex on the surface of the membrane according to previously published H/D exchange data.[22]

Supplementary Tables

Table S1. Fatty acid distribution in isolated natural phospholipids as a percentage area under the curve determined by GC analysis on derived fatty methyl esters. These results were provided by Avanti® Polar Lipids, Inc. (personal communication).

Name	**16:0**	**18:0**	**18:1**	**18:2**	**20:4**	**22:6**
Egg PA	34.2	11.5	31.5	18.5	2.7	0.7
Egg PC	32.7	12.3	32.0	17.1	2.7	0.0
Egg PE	17.3	24.2	18.1	14.0	16.0	4.2
Egg PG	32.9	12.2	30.2	18.7	3.5	0.0
Brain PS	0.0	42.0	30.0	0.0	2.0	11.0

References

1. Dessen, A.; Tang, J.; Schmidt, H.; Stahl, M.; Clark, J.; Seehra, J.; Somers, W., *Cell* **1999,** *97*, 349-360.
2. Mouchlis, V. D.; Bucher, D.; McCammon, J. A.; Dennis, E. A., *PNAS* **2015,** *112*, E516-E525.
3. Jacobson, M. P.; Pincus, D. L.; Rapp, C. S.; Day, T. J.; Honig, B.; Shaw, D. E.; Friesner, R. A., *Proteins* **2004,** *55*, 351-67.
4. Mouchlis, V. D.; Limnios, D.; Kokotou, M. G.; Barbayianni, E.; Kokotos, G.; McCammon, J. A.; Dennis, E. A., *J. Med. Chem.* **2016,** *59*, 4403-4414.
5. Mouchlis, V. D.; Morisseau, C.; Hammock, B. D.; Li, S.; McCammon, J. A.; Dennis, E. A., *Bioorg. Med. Chem.* **2016,** *24*, 4801-4811.
6. Friesner, R. A.; Murphy, R. B.; Repasky, M. P.; Frye, L. L.; Greenwood, J. R.; Halgren, T. A.; Sanschagrin, P. C.; Mainz, D. T., *J. Med. Chem.* **2006,** *49*, 6177-6196.
7. Wu, E. L.; Cheng, X.; Jo, S.; Rui, H.; Song, K. C.; Davila-Contreras, E. M.; Qi, Y.; Lee, J.; Monje-Galvan, V.; Venable, R. M.; Klauda, J. B.; Im, W., *J Comput Chem* **2014,** *35*, 1997-2004.
8. Lee, J.; Cheng, X.; Swails, J. M.; Yeom, M. S.; Eastman, P. K.; Lemkul, J. A.; Wei, S.; Buckner, J.; Jeong, J. C.; Qi, Y.; Jo, S.; Pande, V. S.; Case, D. A.; Brooks, C. L., 3rd; MacKerell, A. D., Jr.; Klauda, J. B.; Im, W., *J Chem Theory Comput* **2016,** *12*, 405-13.
9. van Meer, G.; Voelker, D. R.; Feigenson, G. W., *Nat. Rev. Mol. Cell Biol.* **2008,** *9*, 112-124.
10. Shirai, Y.; Balsinde, J.; Dennis, E. A., *Biochim. Biophys. Acta* **2005,** *1735*, 119-129.
11. Song, H.; Bao, S.; Lei, X.; Jin, C.; Zhang, S.; Turk, J.; Ramanadham, S., *Biochim. Biophys. Acta* **2010,** *1801*, 547-58.
12. Williams, S. D.; Gottlieb, R. A., *Biochem. J.* **2002,** *362*, 23-32.
13. Humphrey, W.; Dalke, A.; Schulten, K., *J. Mol. Graph.* **1996,** *14*, 33-38.
14. Phillips, J.; Braun, R.; Wang, W.; Gumbart, J.; Tajkhorshid, E.; Villa, E.; Chipot, C.; Skeel, R.; Kalé, L.; Schulten, K., *J. Comput. Chem.* **2005,** *26*, 1781-1802.
15. Adelman, S. A., *J. Chem. Phys.* **1976,** *64*, 2375-2388.
16. Feller, S. E.; Zhang, Y.; Pastor, R. W.; Brooks, B. R., *J. Chem. Phys.* **1995,** *103*, 4613-4621.
17. Jean-Paul, R.; Giovanni, C.; Herman, J. C. B., *J. Comput. Phys.* **1977,** *23*, 327-341.
18. Ulrich, E.; Lalith, P.; Max, L. B.; Tom, D.; Hsing, L.; Lee, G. P., *J. Chem. Phys.* **1995,** *103*, 8577-8593.

19. Vanommeslaeghe, K.; Hatcher, E.; Acharya, C.; Kundu, S.; Zhong, S.; Shim, J.; Darian, E.; Guvench, O.; Lopes, P.; Vorobyov, I.; Mackerell, A. C., *J Comput. Chem.* **2009,** *31*, 671-690.
20. Klauda, J. B.; Venable, R. M.; Freites, J. A.; O'Connor, J. W.; Tobias, D. J.; Mondragon-Ramirez, C.; Vorobyov, I.; MacKerell, A. D.; Pastor, R. W. C., *J. Phys. Chem. B* **2010,** *114*, 7830-7843.
21. Durrant, J. D.; de Oliveira, C. A.; McCammon, J. A., *J. Mol. Graph. Model.* **2011,** *29*, 773-6.
22. Burke, J. E.; Karbarz, M. J.; Deems, R. A.; Li, S.; Woods, V. L., Jr.; Dennis, E. A., *Biochemistry* **2008,** *47*, 6451-9.